PCCP

PAPER

View Article Online
View Journal | View Issue

Cite this: *Phys. Chem. Chem. Phys.*, 2014, **16**, 3230

Catalyst and electrolyte synergy in Li–O_2 batteries†

Forrest S. Gittleson,[a] Ryan C. Sekol,[a] Gustavo Doubek,[ab] Marcelo Linardi[b] and André D. Taylor*[a]

Received 28th October 2013,
Accepted 14th December 2013

DOI: 10.1039/c3cp54555e

www.rsc.org/pccp

Understanding the interactions between catalyst and electrolyte in Li–O_2 systems is crucial to improving capacities, efficiencies, and cycle life. In this study, supported noble metal catalysts Pt/C, Pd/C, and Au/C were paired with popular Li–O_2 electrolyte solvents dimethoxyethane (DME), tetraglyme (TEGDME), and dimethyl sulfoxide (DMSO). The effects of these combinations on stability, kinetics, and activity were assessed. We show evidence of a synergistic effect between Pt and Pd catalysts and a DMSO-based electrolyte which enhances the kinetics of oxygen reduction and evolution reactions. DME and TEGDME are more prone to decomposition and less kinetically favorable for oxygen reduction and evolution than DMSO. While the order of oxygen reduction onset potentials with each catalyst was found to be consistent across electrolyte (Pd > Pt > Au), larger overpotentials with DME and TEGDME, and negative shifts in onset after only five cycles favor the stability of a DMSO electrolyte. Full cell cycling experiments confirm that catalyst–DMSO combinations produce up to 9 times higher discharge capacities than the same with TEGDME after 20 cycles (~707.4 *vs.* 78.8 mA h g^{-1} with Pd/C). *Ex situ* EDS and *in situ* EIS analyses of resistive species in the cathode suggest that improvements in capacity with DMSO are due to a combination of greater electrolyte conductivity and catalyst synergies. Our findings demonstrate that co-selection of catalyst and electrolyte is necessary to exploit chemical synergies and improve the performance of Li–O_2 cells.

Introduction

The lithium–oxygen cell is an attractive technology for the next generation of rechargeable batteries because of its high theoretical energy density (11 686 W h kg^{-1}) as compared to standard lithium-ion cells.[1,2] Though the rechargeability of Li–O_2 cells was first established by Abraham and Jiang in 1996,[3] many design challenges must still be addressed before widespread adoption. Among these, selection and accompanying characterization of suitable oxygen electrode materials and electrolytes is of primary importance.

Careful selection of oxygen electrode materials and their morphology is necessary to promote cyclability while enabling higher charge rates. Porous carbon remains a common oxygen electrode in Li–O_2 cells, but exhibits relatively poor round trip efficiency when cycled and has been shown to degrade, forming irreversible species.[4] Recent literature has suggested that incorporating catalysts into a porous carbon matrix can increase the round trip efficiency of a Li–O_2 cell and enhance its cycle life.[5–10] Catalysts of this nature serve two purposes: to reduce the overpotential between the oxygen reduction (ORR) and oxygen evolution (OER) reactions and to promote cathode cyclability by facilitating removal of the solid discharge product upon charging. Pt, Pd, and Au have previously been shown to catalyze ORR and OER,[6,9] and an oxygen electrode of microporous Au has demonstrated remarkably stable cycling over 100 cycles when paired with a DMSO-based electrolyte.[11] Combining Pt and Au in a bimetallic catalyst has even been able to achieve a record round trip efficiency of 73%,[12] though efficiencies in excess of 90% are seen to be necessary for practical application.[13] Metallic oxide catalysts such as Co_3O_4[14,15] and Pb–Ru–O[16] have also been utilized to improve cycle stability. Despite these findings, the use of catalysts has recently been questioned because of a presumed inability to reduce the overpotential of oxygen evolution reactions.[17] The results presented here demonstrate that catalysts *do* affect oxygen reduction and evolution kinetics and activity, and that proper pairing with non-aqueous electrolytes is essential to realize those benefits.

Some criteria for selecting suitable non-aqueous liquid electrolytes include low volatility, good lithium-ion conductivity,

[a] *Department of Chemical and Environmental Engineering, Yale University, 9 Hillhouse Ave, New Haven, CT, USA. E-mail: andre.taylor@yale.edu*
[b] *Hydrogen and Fuel Cell Center, Nuclear and Energy Research Institute - IPEN/CNEN - SP. Av. Prof. Lineu Prestes, 2242, Cidade Universitária, 05508-000 São Paulo - SP, Brazil*

† Electronic supplementary information (ESI) available: Supporting figures, referenced in the text. See DOI: 10.1039/c3cp54555e

and high oxygen solubility. Most recent studies employing non-aqueous electrolyte solvents have utilized dimethoxyethane (DME), tetraglyme (TEGDME), and, increasingly, dimethyl sulfoxide (DMSO).[18–20] Much literature has shown that carbonate solvents, including propylene carbonate and ethylene carbonate are unsuitable due to side reactions that generate irreversible products.[20–24] Ethers like DME and TEGDME are more stable, but may exhibit high volatility, decreased ion conductivity, and will still decompose to form undesired products.[17,20,25–28] Recent studies employing DMSO demonstrate significant improvements in capacity and cycle life[11,29–32] and may support the increased use of this electrolyte.

While most literature evaluating Li–O_2 systems demonstrates novel oxygen electrode architectures and electrolyte combinations in cells for practical galvanostatic cycling, studies that investigate the interplay between catalyst and electrolyte are few. Existing literature has sought to study the function of different catalysts in a single electrolyte (DME) or to evaluate the effect of electrolyte with one or two different oxygen electrode materials. Here we present the first report on the effects and consequences of catalyst and electrolyte co-selection. Supported noble metal catalyst performance was studied as a function of pairing with the most common non-aqueous electrolyte solvents: DME, TEGDME and DMSO. Our findings indicate that kinetics and catalyst activity are selectively enhanced through the use of a DMSO-based electrolyte. Not only is DMSO more stable than DME and TEGDME when paired with noble metal catalysts, but it yields higher oxygen reduction onset potentials, increased oxygen evolution activities, and higher discharge capacities when used in a full cell. This study also constitutes the first evaluation of a Li–O_2 system to employ a DMSO-based electrolyte with Pt and Pd containing catalysts, and to use combined ORR and OER cycling analysis to shed light on the consequences of joint catalyst–electrolyte selection.

Experimental

Materials

Carbon (XC-72) supported catalysts consisted of 20% by weight of Pt (BASF), Pd and Au (Premetek). Reagent grade $LiClO_4$ (Sigma Aldrich) was used as the electrolyte salt. Anhydrous dimethoxyethane (Sigma Aldrich), tetraglyme (Sigma Aldrich), and anhydrous dimethyl sulfoxide (Alfa Aesar) were used as electrolyte solvents and stored in argon or nitrogen purged glove boxes. Nafion solution (5% in alcohol) (Ion Power) was mixed into catalyst inks.

Electrode/cell preparation

For rotating disc electrode experiments, a three electrode cell was used with 50 mL of electrolyte and a sealed Li/Li^+ reference electrode. All 0.1 M $LiClO_4$ electrolytes and fresh reference electrodes were prepared inside an isolated glove box. Pt mesh was used as the counter electrode and a 5 mm diameter glassy carbon electrode was used as the working electrode. Upon removal from the glove box, solutions were immediately purged with either dry He or dry O_2 for at least 15 minutes.

Ink solutions of standard catalysts were prepared with 12.5 mg of catalyst in a mixture of 2 mL DI water and 3 mL isopropyl alcohol with 20 μL of Nafion solution. Inks were sonicated thoroughly before use. 10 μL of ink solution was added to the glassy carbon and dried. Upon immersion in electrolyte solution, the electrode was rotated at 900 rpm. Cyclic voltammetry experiments employed a BioLogic VSP potentiostat for scans in voltage ranges selected for each electrolyte.

Full cell evaluation

An airtight test cell based on a previously reported design[7] was used for galvanostatic cycling of 12.7 mm diameter oxygen electrodes. A 11.1 mm diameter disc of Li-foil was used as the anode to a flattened Ni-foam oxygen electrode with approximately 40 μg of supported catalyst or XC-72 control. A 13 mm Whatman glass fiber filter impregnated with electrolyte was used as the separator. Cells were sealed in an Ar-filled glovebox and allowed to age for approximately 12 hours prior to purging with dry O_2. O_2 pressure was approximately 20 psig. All galvanostatic cycling was conducted at a rate of 50 μA. Electrochemical impedance spectroscopy (EIS) measurements with an amplitude of 50 mV and a range of 10^5–0.1 Hz were conducted using a BioLogic potentiostat channel following the discharge and charge scans of cycles 1, 5, 10, and 20.

Physical characterization

Standard catalyst morphology was verified using an FEI Tecnai Osiris 200 kV transmission electron microscope (TEM) (Fig. S1†). Visual characterization and quantification of atomic species on Ni-foam deposited oxygen electrodes was conducted using a Hitachi SU-70 scanning electron microscope (SEM) with energy dispersive X-ray spectroscopy (EDS) function.

Electrolyte stability and kinetics

Rotating disc electrode cyclic voltammetry (CV) and polarization techniques are ideal for evaluating Li–O_2 reactions and have been employed before.[18,30,33–35] In this study, the activities of supported catalysts deposited onto a glassy carbon (GC) electrode and immersed in a 0.1 M $LiClO_4$ electrolyte were evaluated using CV. Purging the electrolyte with either inert He or dry O_2 prior to experiments ensured either a dearth of oxygen or oxygen saturation of the solution.

A 5 mm GC working electrode was used to determine the baseline stability of electrolytes with a carbon electrode. Rotating disc cyclic voltammetry was conducted following purging with He in the range 1.0–4.5 V (Fig. 1 in red). Electrolyte solvents DME and TEGDME exhibit reaction peaks beginning at 2.4 and 2.3 V in the discharge scan and above 4.0 V in the charge scan, respectively. As the solutions are free of O_2, we expect these represent electrolyte decomposition reactions. DMSO exhibits no distinct peaks over the entire range, suggesting good stability with glassy carbon, consistent with a previous result.[30] With these findings and support from existing literature,[18] potential ranges 1.5–4.0 V for DME and TEGDME electrolytes

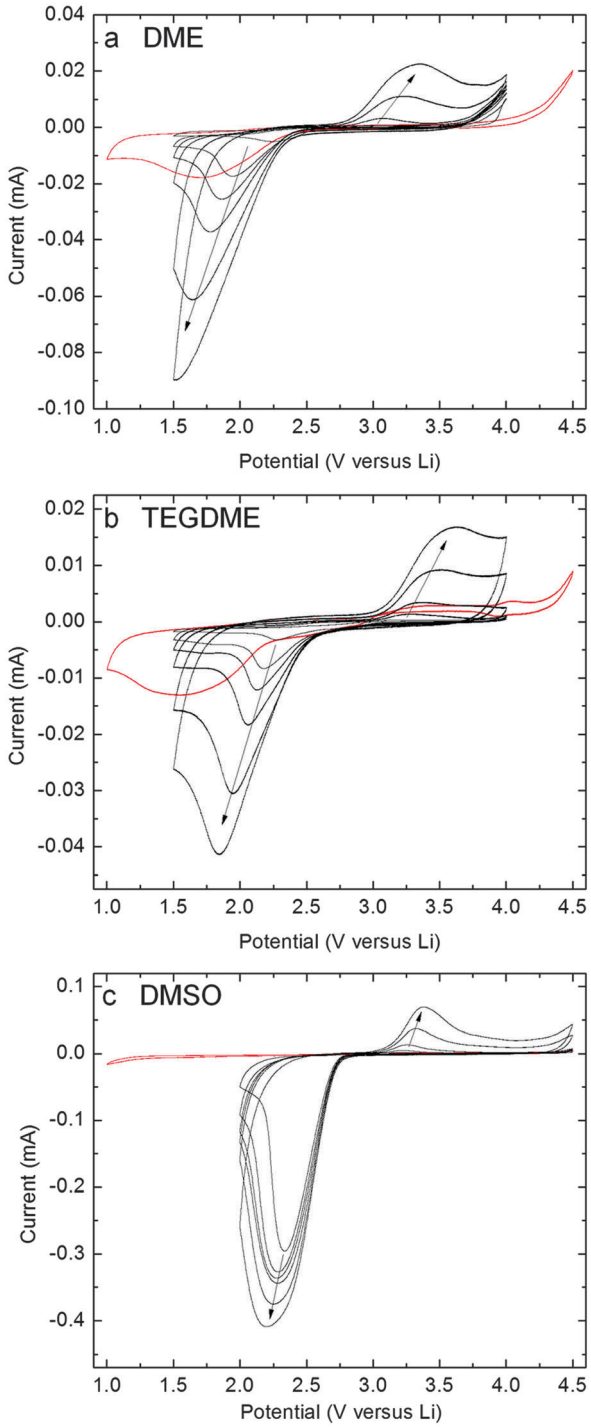

Fig. 1 CV of glassy carbon electrode in (a) DME, (b) TEGDME and (c) DMSO at increasing scan rates 1, 5, 10, 20, 50, 100 mV s^{-1} (denoted by arrows) under O_2 atmosphere (black) and at 20 mV s^{-1} under He atmosphere (red).

and 2.0–4.5 V for a DMSO electrolyte were selected for evaluation in an O_2 atmosphere.

All electrolytes were purged with dry O_2 before cyclic voltammetry at rates of 1, 5, 10, 20, 50, and 100 mV s^{-1} (Fig. 1 in black). Differences in the height and position of peaks at certain rates can be used to compare the activity and kinetics

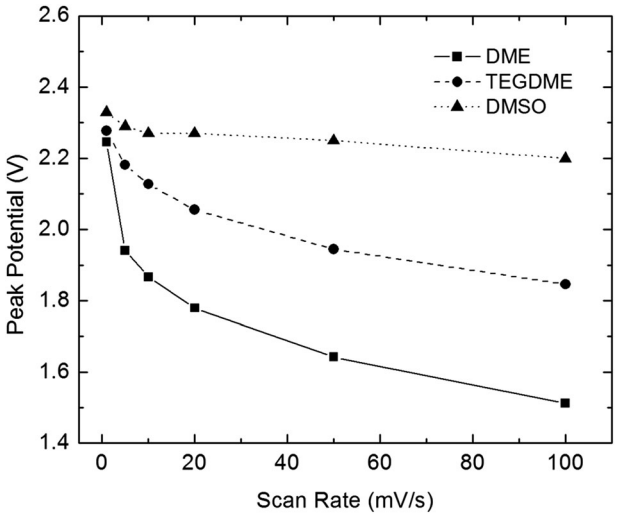

Fig. 2 Oxygen reduction peak potentials *versus* scan rate for a glassy carbon electrode in each electrolyte.

of reactions in each electrolyte. We find that based upon peak height alone, the oxygen reduction activity of GC is greater in DMSO than in DME or TEGDME. This is consistent with the Li^+ conductivity of each electrolyte, but not with the oxygen solubility (Table S1†).[18] Furthermore, as scan rates are increased, exponential increases in peak heights and negative shifts in peak potentials denote the slower kinetics of ORR and OER in DME and TEGDME compared to DMSO. While these findings may suggest a diffusion limited process with DME and TEGDME, the diffusion coefficient of Li^+ is greater in DME than DMSO (Table S1†), thus reaction kinetics are a more likely culprit. A summary of ORR peak potentials *vs.* scan rate is shown in Fig. 2 and demonstrates that negative shifts are quite significant (approximately 0.7 and 0.4 V for DME and TEGDME, respectively). The theory that DMSO better stabilizes the superoxide intermediate for oxygen reduction due to its higher donor number,[18] is supported by this result. The peak potential of oxygen evolution upon reverse scan also exhibits distinct behavior with each electrolyte (Fig. 1). DME and DMSO both exhibit oxygen evolution peak potentials of approximately 3.4 V while TEGDME has a peak potential closer to 3.6 V at the fastest scan rate (100 mV s^{-1}). This data collectively suggest that the adoption of a DMSO-based electrolyte should allow for increased cycling rates and decreased overpotentials in standard cells.

Catalyst–electrolyte pairing

In order to promote catalysis of oxygen reduction and evolution reactions, an appropriate selection of stable, conductive electrolyte solvent is necessary. Fig. 3a–c shows CV scans of a bare GC electrode as well as Pt/C, Pd/C, and Au/C on a rotating GC disc under an inert He atmosphere. In this figure, DME and TEGDME exhibit sloping reaction peaks below 2.0 V in the discharge scan for all supported catalysts, corresponding to decomposition reactions. The charge scans with Pt/C and Pd/C electrodes in DME and TEGDME also exhibit various reactions above 3.0 V.

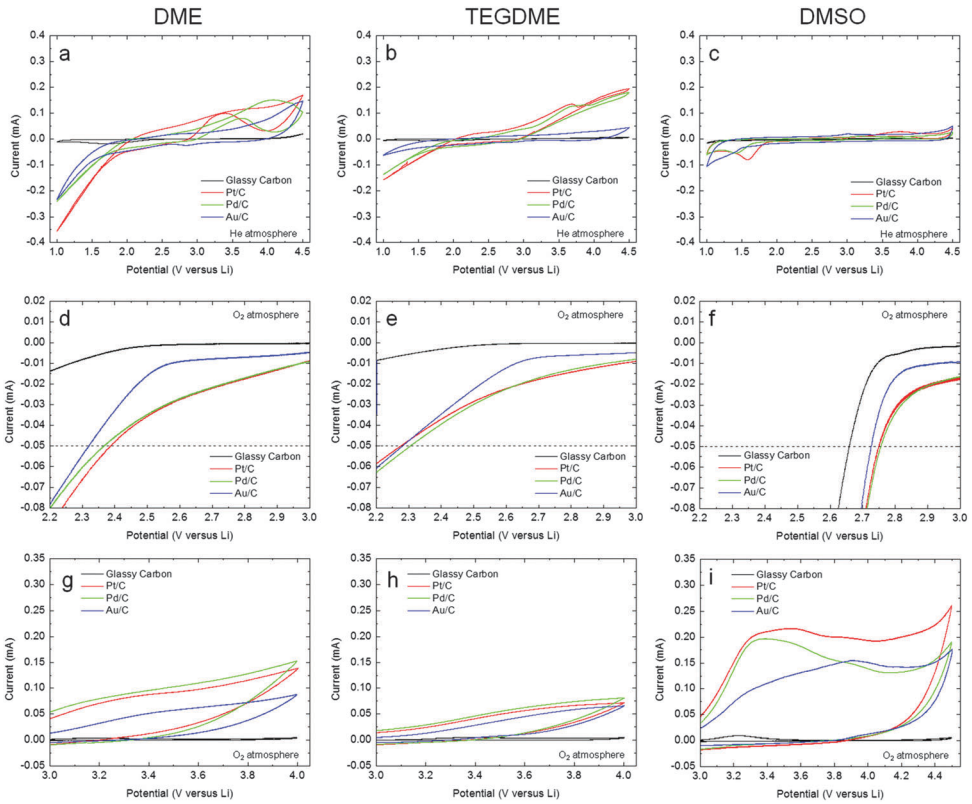

Fig. 3 CV of four catalysts in DME, TEGDME, and DMSO-based electrolytes. (a–c) Stability of electrolyte solvents with catalyst under inert He atmosphere, (d–f) the oxygen reduction onset region during discharge under O_2 atmosphere, (g–i) the oxygen evolution region during charge under O_2 atmosphere. All scans at 20 mV s^{-1}.

While such reactions are likely undesirable, these voltage ranges are unavoidable in the normal operation of a Li–O_2 cell. The DMSO electrolyte exhibits relatively flat profiles for each catalyst except below 2.0 V. Minor reaction peaks for Pt/C and Pd/C in DMSO are also apparent around 3.8 V, but on the whole, DMSO is a more stable solvent than DME or TEGDME with all catalyst samples.

Profiles of the ORR onset region in the second cycle for each catalyst–electrolyte pair are given in Fig. 3d–f. The data shows the average oxygen reduction onset potential in DMSO ($\sim$2.75 V) to be significantly higher than in DME ($\sim$2.35 V) or TEGDME ($\sim$2.30 V). Higher onset potentials with DMSO denote more favorable kinetics which may be attributed to improved charge transfer (see Tafel analysis, Tables S2–S4†). A further analysis of onset potentials over 5 CV scans is given in Fig. 4 and indicates that there are significant shifts with certain catalyst–electrolyte pairs. On average, catalyst onset potentials shift negatively $\sim$0.15 V in DME and TEGDME, and $<$0.05 V in DMSO over 5 cycles. Thus, DMSO both improves the onset potentials of catalyst systems and enhances their stability upon repeated cycling. The order of first cycle onsets is Pd > Pt > Au for each electrolyte, in agreement with previous literature using only a DME-based electrolyte.[6] Pd/C and Pt/C are more negatively affected by continued cycling than Au/C as there is a reordering and/or converging of onset potentials in later cycles. These negative shifts are believed to be due to the formation of irreversible products which deactivate the catalyst surface.

Fig. 3g–i portrays the oxygen evolution region of the second CV scan for all catalyst–electrolyte pairs. The activity of each system is most affected by the electrolyte selection rather than catalyst, with DMSO being the most active followed by DME and TEGDME. The position of oxygen evolution peaks, though subtle, indicates that the major reactions occur around 3.4 V in DME and DMSO and 3.6 in TEGDME. The lack of distinguishing oxygen evolution features with DME and TEGDME do not allow us to parse the expected reactions. That these reactions are well defined in Fig. 3i is consistent with our other results indicating improved kinetics with DMSO and allow us to assign expected reactions. Subtle shifts in slope indicate that in the DMSO case with Pt/C and Pd/C there are reactions occurring at approximately 3.3 V, 3.6 V, and 3.8 V. The latter may be assigned to DMSO degradation as similar behavior is seen at this potential under an inert atmosphere. The most likely reactions occurring at 3.3 V and 3.6 V are those suggested in recent mechanistic papers[36,37] and supported by *in situ* TEM imaging.[38] According to this theory, at lower potentials oxygen evolution occurs at the outer surface of the Li_2O_2 crystal, while further evolution of the bulk occurs at higher potentials. There is some suggestion in the literature of Li_2O formation and decomposition with Pt/C and potentially other catalysts, but the formation of Li_2O during discharge has not been confirmed[34,39] and is

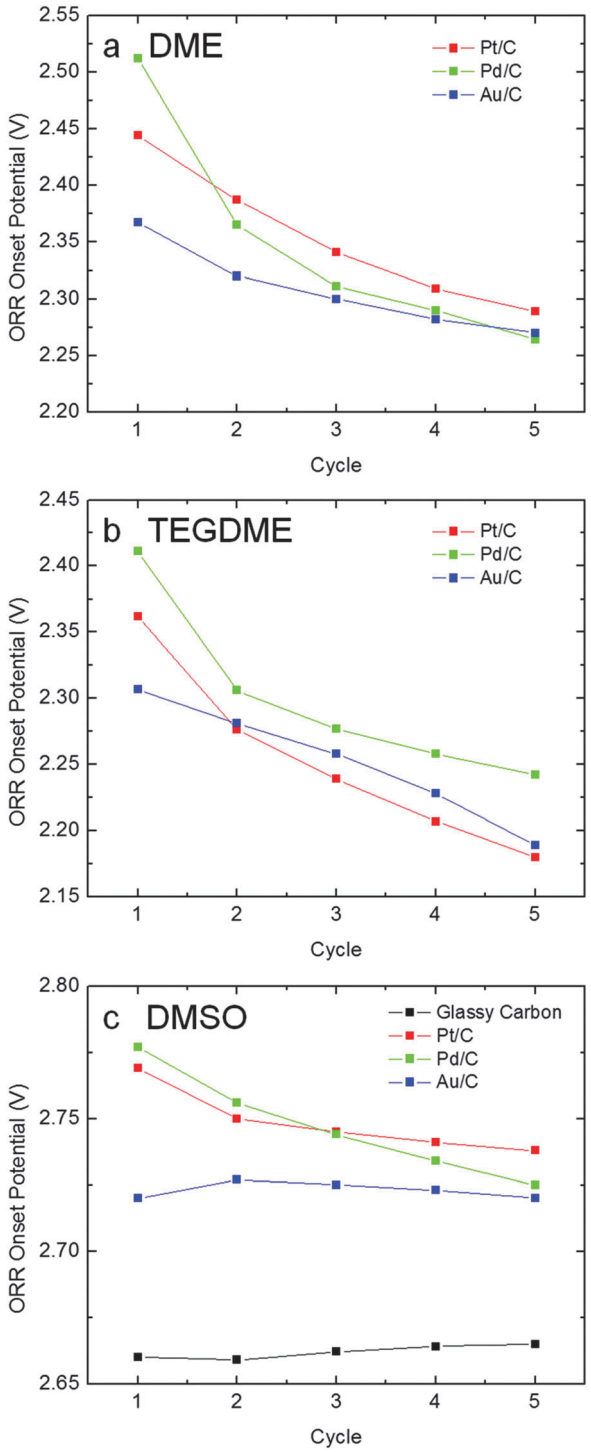

Fig. 4 Shifts in oxygen reduction onsets over 5 CV cycles for each catalyst–electrolyte pair.

not expected. While the mechanism of oxygen evolution may differ from the generally accepted direct reaction on catalyst surfaces,

$$Li_2O_2 \rightarrow O_2 + 2Li^+ + 2e^-,$$

additional studies that exclude the presence of carbon and seek to detect *in situ* surface species are necessary.

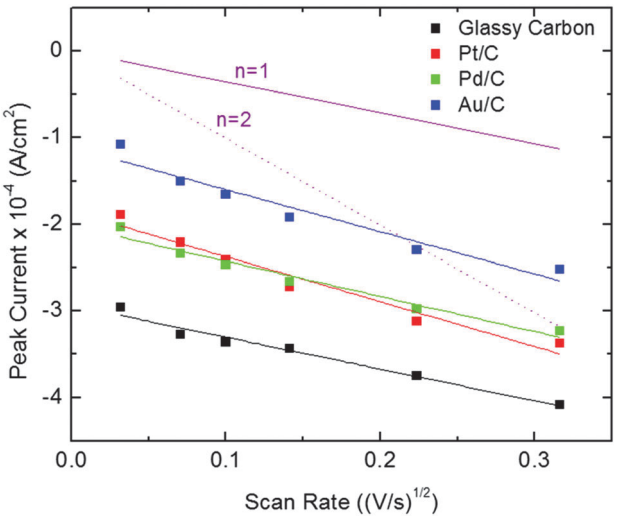

Fig. 5 Nicholson and Shain plot of peak currents *versus* the square root of scan rate for standard catalysts in a DMSO-based electrolyte.

The rate limiting step of oxygen reduction with standard catalysts can be electrochemically distinguished without the difficulty of *in situ* studies. For an irreversible electrochemical reaction, the peak current and scan rates of CVs may be related according to the Nicholson and Shain relationship:[18,30,33,35]

$$I_p = (2.99 \times 10^5) n^{3/2} \alpha^{1/2} A C D^{1/2} V^{1/2}$$

Here I_p is the peak current, n, the number of electrons transferred, α, a correction factor for irreversibility, A, the electrode area, C, the oxygen concentration in solution, D, the diffusion coefficient of O_2, and V, the scan rate. A fitting of our data for the DMSO system (Fig. S2†) to a model slope from an idealized mechanism of 1 or 2 electrons with $\alpha = 0.8$ is provided in Fig. 5. The findings support a one electron limiting reaction for oxygen reduction with all catalysts in a DMSO electrolyte and is consistent with previous literature using a glassy carbon electrode.[18,30] We conclude that despite having more favorable onset potentials and reaction kinetics, the rate limiting step of oxygen reduction, the formation of the superoxide (O_2^-) radical, is not affected by the catalysts used in this study. Expanding this analysis to DME and TEGDME-based electrolytes was unsuccessful due to the negative potential shift of ORR peaks at higher scan rates.

Full cell evaluation

By employing full cell cycling we are able to support many of the conclusions drawn through rotating disc cyclic voltammetry. Oxygen electrodes consisting of flattened Ni-foam were impregnated and dried with approximately 40 μg of Pt/C, Pd/C or Au/C and assembled into cells opposite a Li-foil anode. Galvanostatic cycling with catalysts and a carbon black (XC-72) standard was conducted with TEGDME and DMSO electrolytes while DME was excluded due to its high volatility. Discharge capacities over 20 cycles are presented in Fig. 6, normalized by

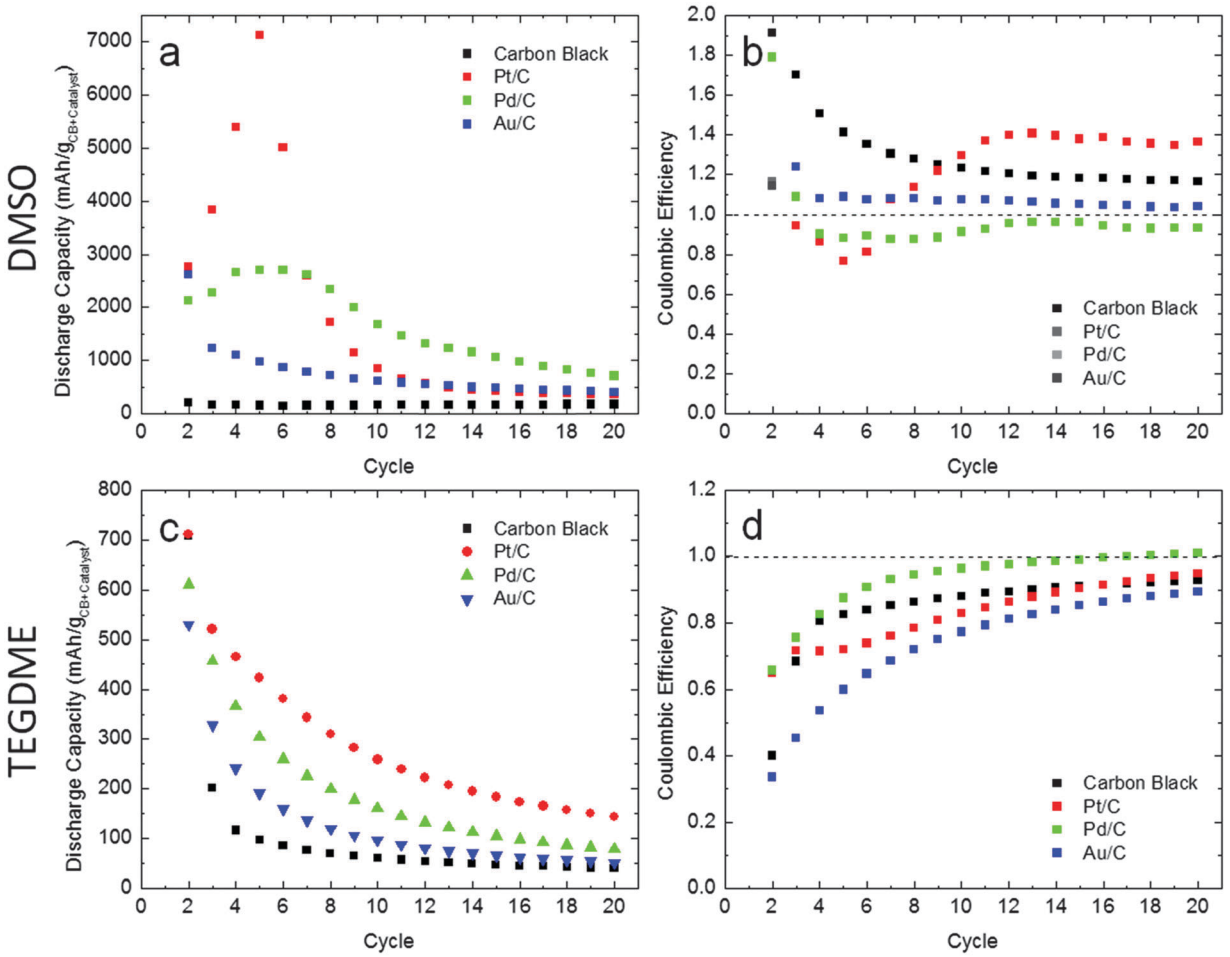

Fig. 6 Discharge capacity of standard catalysts on Ni-foam with TEGDME and DMSO-based electrolytes cycled at 50 μA with accompanying coulombic efficiency.

the total weight of carbon and catalyst, along with coulombic efficiencies. The first cycle is excluded from our analysis due to significant variation and instead we focus on the stability of discharge over 20 cycles. We find that discharge capacity for all samples is greater in DMSO than in TEGDME at the same 50 μA rate. While all samples decrease in capacity upon repeated cycling, catalyst samples in DMSO better retain their enhanced capacity over the control at the 20th cycle (values available in Table S5†). Coulombic efficiencies for DMSO samples are slightly greater than 1.0 for several samples indicating the presence of parasitic reactions in the charge scan (especially prevalent for Pt/C). These reactions appear to occur in the range of 3.8–4.5 V, but mostly over 4.2, as in Fig. 3i. Optimization of cycling parameters should help eliminate these side reactions in future studies. Coulombic efficiencies below 1.0 for samples in TEGDME suggest that the discharge scan is more robust than the charge scan, indicating the production of irreversible discharge products with this electrolyte. This result is expected based on the stability analysis in Fig. 3b. In accordance with our prior findings, Pt/C and Pd/C catalysts perform better in both electrolytes (at least in initial cycles) than Au/C or the baseline. Pairing Pd/C with DMSO results in a discharge capacity 9 times greater at the 20th cycle than the same paired with TEGDME (707.4 *vs.* 78.8 mA h $g_{Pd/C}^{-1}$).

All electrodes were removed from cells and rinsed with isopropyl alcohol following the 20th charge cycle and analyzed

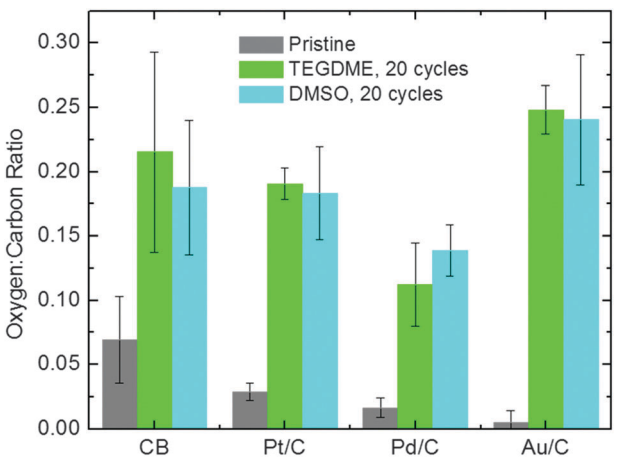

Fig. 7 Relative oxygen : carbon ratio before and after 20 cycles at a 50 μA rate for each catalyst in TEGDME and DMSO-based electrolytes.

by SEM (Fig. S3†) and EDS. While nanoparticle deposition (Li_2O_2 or other species) on the carbon black support is difficult to detect by SEM, EDS results indicate changes in the oxygen content of the electrode. Fig. 7 presents an analysis of oxygen : carbon ratio quantified by multiple point analysis on the carbon black support for all samples. A significant increase in oxygen content after cycling is expected with both DMSO and TEGDME electrolytes due to the formation of irreversible products or incomplete oxygen evolution. The oxygen content is similar in both electrolytes and across catalysts which suggests that the buildup of (resistive) oxygen containing species is not the main impeder of cathode cyclability with TEGDME. The exact species present could not be determined by other *ex situ* methods due to the low loading of carbon and catalyst. We believe, however, that the presence of carbon is a confounding factor to further analysis; thus determining selectivity in discharge products due to catalyst would most likely necessitate carbon-free oxygen electrodes.

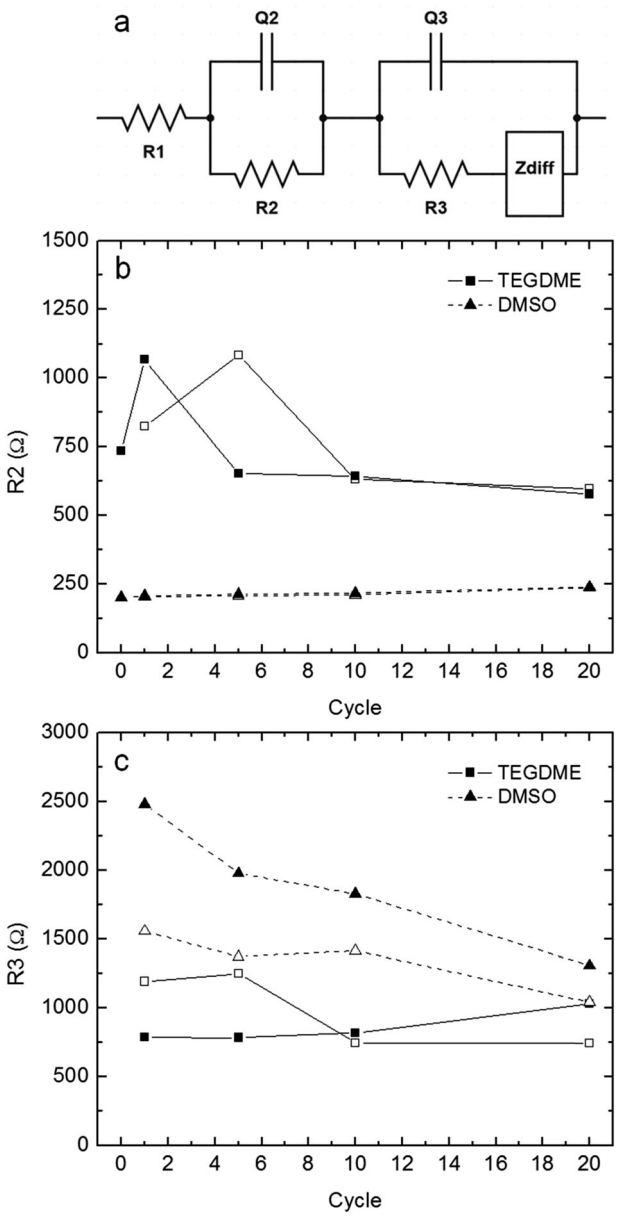

Fig. 8 (a) Circuit diagram for fitting of EIS data and (b, c) graphical representation of EIS fit parameters of charge (open symbols) and discharge (closed symbols) for a carbon black on Ni-foam electrode with TEGDME and DMSO-based electrolytes.

Electrochemical impedance spectroscopy was conducted on control samples of carbon black to better understand changes occurring over repeated cycling with TEGDME and DMSO electrolytes. The impedance of cells was measured before cycling and after the discharge and charge of cycles 1, 5, 10, and 20. The data was fitted according to the circuit diagram in Fig. 8a. In this diagram, R1 represents the resistance of the wires, cell, and electrolyte, although the electrolyte resistance is dominant. The element consisting of Q2 and R2 functions as a model for the anode and the element consisting of Q3, R3, and Zdiff functions as a model for the cathode. Model fits for R1 give relatively consistent values of approximately 12 Ω for DMSO and 120–140 Ω for TEGDME. The evolution of fitting parameters R2 and R3 for the carbon black and electrolyte system are presented in Fig. 8b and c, demonstrating the change in electrode resistances. To obtain a reasonable fitting of the results, the constant phase elements Q2 and Q3 were chosen to have magnitudes of 10^{-6} and 10^{-3} F $s^{(\alpha-1)}$, respectively, where α is a fitting parameter to account for the variation from capacitive behavior. Such non-ideality is likely due to a distribution of charges and non-uniform electrode surfaces. A recent report cites similar capacitive magnitudes as pertaining to anode and cathode.[40] Our fitting of R2 indicates that the Li-foil anode is more resistive in the TEGDME electrolyte. The evolution of R3 shows higher cathode resistances with DMSO *vs.* TEGDME, but the resistance following the 20th cycle is close for both cells. This agrees with our evaluation of oxygen-containing resistive species in Fig. 7. When combined with the charge–discharge results in Fig. 6 for a carbon black electrode, this impedance data implies that cathode resistance is not the most important factor affecting discharge capacity with TEGDME and DMSO electrolytes. Instead, higher anode and electrolyte resistances with TEGDME and kinetic synergies in catalyst–DMSO systems may collectively account for the enhanced performance of DMSO-containing cells.

Conclusion

In this work, DME-, TEGDME- and DMSO-based Li–O_2 electrolytes were evaluated on the basis of electrochemical stability, kinetics, and their synergy with supported metal catalysts. DMSO was found to be more kinetically favorable and stable than DME and TEGDME when paired with noble metal catalysts Pt, Pd, and Au. An analysis under O_2 atmosphere showed that oxygen reduction onset potentials follow an order that is consistent across electrolyte (Pd > Pt > Au) but that negative shifts in onset with cycling favor the stability of a DMSO electrolyte. Oxygen evolution reactions are also more favorable in a DMSO electrolyte and are enhanced by Pt and Pd catalysts. These findings extend to full cell cycling where cells with a DMSO electrolyte exhibited higher discharge capacities than

those with TEGDME. When paired with DMSO, Pt, Pd, and Au catalysts displayed significantly higher discharge capacities than the baseline carbon. These results champion the use of DMSO as a stable and kinetically favorable electrolyte that enhances the activity of noble metal catalysts.

Acknowledgements

The authors would like to acknowledge that support for this work came from the Semiconductor Research Corporation 2011-RJ-21516 and National Science Foundation NSF-CBET-0954985 CAREER Award. Facilities use was supported by YINQE and NSF MRSEC DMR 1119826 (CRISP).

References

1 P. Bruce, S. Freunberger, L. Hardwick and J. Tarascon, *Nat. Mater.*, 2012, **11**, 19–30.
2 G. Girishkumar, B. McCloskey, A. C. Luntz, S. Swanson and W. Wilcke, *J. Phys. Chem. Lett.*, 2010, **1**, 2193–2203.
3 K. M. Abraham and Z. Jiang, *J. Electrochem. Soc.*, 1996, **143**, 1–5.
4 M. M. O. Thotiyl, S. A. Freunberger, Z. Peng and P. G. Bruce, *J. Am. Chem. Soc.*, 2013, **135**, 494–500.
5 Y.-C. Lu, D. G. Kwabi, K. P. C. Yao, J. R. Harding, J. Zhou, L. Zuin and Y. Shao-Horn, *Energy Environ. Sci.*, 2011, **4**, 2999–3007.
6 Y.-C. Lu, H. A. Gasteiger and Y. Shao-Horn, *J. Am. Chem. Soc.*, 2011, **133**, 19048–19051.
7 Y.-C. Lu, H. A. Gasteiger, M. C. Parent, V. Chiloyan and Y. Shao-Horn, *Electrochem. Solid-State Lett.*, 2010, **13**, A69–A72.
8 Y. Shao, S. Park, J. Xiao, J. Zhang, Y. Wang and J. Liu, *ACS Catal.*, 2012, **2**, 844–857.
9 J. R. Harding, Y.-C. Lu, Y. Tsukada and Y. Shao-Horn, *Phys. Chem. Chem. Phys.*, 2012, **14**, 10540–10546.
10 J. Yin, B. Fang, J. Luo, B. Wanjala, D. Mott, R. Loukrakpam, M. S. Ng, Z. Li, J. Hong, M. S. Whittingham and C.-J. Zhong, *Nanotechnology*, 2012, **23**, 305404.
11 Z. Peng, S. A. Freunberger, Y. Chen and P. G. Bruce, *Science*, 2012, **337**, 563–566.
12 Y.-C. Lu, Z. Xu, H. A. Gasteiger, S. Chen, K. Hamad-Schifferli and Y. Shao-Horn, *J. Am. Chem. Soc.*, 2010, **132**, 12170–12171.
13 J. Christensen, P. Albertus, R. S. Sanchez-Carrera, T. Lohmann, B. Kozinsky, R. Liedtke, J. Ahmed and A. Kojic, *J. Electrochem. Soc.*, 2012, **159**, R1–R30.
14 W. Ryu, T. Yoon, S. H. Song, S. Jeon, Y. Park and I. Kim, *Nano Lett.*, 2013, **13**, 4190–4197.
15 R. Black, J.-H. Lee, B. Adams, C. A. Mims and L. F. Nazar, *Angew. Chem., Int. Ed.*, 2013, **52**, 392–396.
16 S. H. Oh, R. Black, E. Pomerantseva, J.-H. Lee and L. F. Nazar, *Nat. Chem.*, 2012, **4**, 1004–1010.
17 B. D. McCloskey, R. Scheffler, A. Speidel, D. S. Bethune, R. M. Shelby and A. C. Luntz, *J. Am. Chem. Soc.*, 2011, **133**, 18038–18041.
18 C. O. Laoire, S. Mukerjee, K. M. Abraham, E. J. Plichta and M. A. Hendrickson, *J. Phys. Chem. C*, 2010, **114**, 9178–9186.
19 B. McCloskey, D. Bethune, R. Shelby, T. Mori, R. Scheffler, A. Speidel, M. Sherwood and A. Luntz, *J. Phys. Chem. Lett.*, 2012, **3**, 3043–3047.
20 B. D. McCloskey, D. S. Bethune, R. M. Shelby, G. Girishkumar and A. C. Luntz, *J. Phys. Chem. Lett.*, 2011, **2**, 1161–1166.
21 W. Xu, K. Xu, V. V. Viswanathan, S. A. Towne, J. S. Hardy, J. Xiao, Z. Nie, D. Hu, D. Wang and J.-G. Zhang, *J. Power Sources*, 2011, **196**, 9631–9639.
22 W. Xu, V. V. Viswanathan, D. Wang, S. A. Towne, J. Xiao, Z. Nie, D. Hu and J.-G. Zhang, *J. Power Sources*, 2011, **196**, 3894–3899.
23 J. Xiao, J. Hu, D. Wang, D. Hu, W. Xu, G. L. Graff, Z. Nie, J. Liu and J.-G. Zhang, *J. Power Sources*, 2011, **196**, 5674–5678.
24 S. A. Freunberger, Y. Chen, Z. Peng, J. M. Griffin, L. J. Hardwick, F. Bardé, P. Novák and P. G. Bruce, *J. Am. Chem. Soc.*, 2011, **133**, 8040–8047.
25 B. D. McCloskey, A. Speidel, R. Scheffler, D. C. Miller, V. Viswanathan, J. S. Hummelshøj, J. K. Nørskov and A. C. Luntz, *J. Phys. Chem. Lett.*, 2012, **3**, 997–1001.
26 S. A. Freunberger, Y. Chen, N. E. Drewett, L. J. Hardwick, F. Bardé and P. G. Bruce, *Angew. Chem., Int. Ed.*, 2011, **50**, 8609–8613.
27 B. M. Gallant, R. R. Mitchell, D. G. Kwabi, J. Zhou, L. Zuin, C. V Thompson and Y. Shao-Horn, *J. Phys. Chem. C*, 2012, **116**, 20800–20805.
28 S. Meini, N. Tsiouvaras, K. U. Schwenke, M. Piana, H. Beyer, L. Lange and H. A. Gasteiger, *Phys. Chem. Chem. Phys.*, 2013, **15**, 11478–11493.
29 D. Xu, Z.-L. Wang, J.-J. Xu, L.-L. Zhang and X.-B. Zhang, *Chem. Commun.*, 2012, **48**, 6948–6950.
30 M. J. Trahan, S. Mukerjee, E. J. Plichta, M. A. Hendrickson and K. M. Abraham, *J. Electrochem. Soc.*, 2013, **160**, A259–A267.
31 M. M. Ottakam Thotiyl, S. A. Freunberger, Z. Peng, Y. Chen, Z. Liu and P. G. Bruce, *Nat. Mater.*, 2013, **12**, 1050–1056.
32 Y. Chen, S. A. Freunberger, Z. Peng, O. Fontaine and P. G. Bruce, *Nat. Chem.*, 2013, **5**, 489–494.
33 C. O. Laoire, S. Mukerjee, K. M. Abraham, E. J. Plichta and M. A. Hendrickson, *J. Phys. Chem. C*, 2009, **113**, 20127–20134.
34 Y.-C. Lu, H. A. Gasteiger, E. Crumlin, R. McGuire and Y. Shao-Horn, *J. Electrochem. Soc.*, 2010, **157**, A1016–A1025.
35 C. J. Allen, S. Mukerjee, E. J. Plichta, M. A. Hendrickson and K. M. Abraham, *J. Phys. Chem. Lett.*, 2011, **2**, 2420–2424.
36 Y. Lu and Y. Shao-Horn, *J. Phys. Chem. Lett.*, 2013, **4**, 93–99.
37 B. M. Gallant, D. G. Kwabi, R. R. Mitchell, J. Zhou, C. V. Thompson and Y. Shao-Horn, *Energy Environ. Sci.*, 2013, **6**, 2518–2528.
38 L. Zhong, R. R. Mitchell, Y. Liu, B. M. Gallant, C. V. Thompson, J. Y. Huang, S. X. Mao and Y. Shao-Horn, *Nano Lett.*, 2013, **13**, 2209–2214.
39 B. D. McCloskey, R. Scheffler, A. Speidel, G. Girishkumar and A. C. Luntz, *J. Phys. Chem. C*, 2012, **116**, 23897–23905.
40 J. Adams, M. Karulkar and V. Anandan, *J. Power Sources*, 2013, **239**, 132–143.